The other two-center integrals of the form $\langle\alpha^0|G_{1s\alpha}|\beta^0\rangle$ are much more complicated. To determine $G_{1s\alpha}$ from (A12), we must use spheroïdal coordinates centered on nuclei α and β and express all the integrals in terms of elementary ones which we have tabulated. Throughout the whole calculation we have followed the methods of Kotani, Amemiya, and Simose[8] to determine the auxiliary functions. Few of them have been extrapolated from the parameter $\delta R=7$ to 7.6 which is the value for diamond.

3. Numerical Results

We obtain the following values:

$$\begin{aligned}\langle yy\rangle &= -7.739\times10^{-6}\delta^2,\\ \langle yz\rangle &= 197\,355\times10^{-6}\delta^2,\\ \langle vx\rangle &= -267\,231\times10^{-6}\delta^2.\end{aligned}\tag{B22}$$

We notice that $\langle yz\rangle$ and $\langle vx\rangle$ have much higher values than $\langle yy\rangle$. This comes from the fact that for the one-center integrals we have

$$\langle yz\rangle_1=-\langle vx\rangle_1\simeq10\langle yy\rangle_1,\tag{B23}$$

while two-center integrals are of the same order of magnitude in each case. We give (Table III) the energy lowering in each case, in the Hartree-Fock approximation with $\omega_E=\omega_T=2.5\times10^{14}$ rad/sec, maximum optical value of the phonon spectrum.

TABLE III. Energy lowering in the perturbation model. We can see that the energy lowering for a trigonal distortion takes on values which are too large in each case.

Center	Electronic level	ΔE tetragonal eV	ΔE trigonal eV
V^+	$^2T_2$	4.10^{-3}	11.5
V^0	^1E	4.10^{-3}	
	$^3T_1$	3.10^{-3}	9.4
V^-	$^2T_1$	7.10^{-4}	1.5

PHYSICAL REVIEW VOLUME 164, NUMBER 3 15 DECEMBER 1967

Electronic Structure and Optical Properties of Hexagonal CdSe, CdS, and ZnS†

T. K. BERGSTRESSER* AND MARVIN L. COHEN‡
Department of Physics, University of California, Berkeley, California
(Received 26 June 1967)

Pseudopotential form factors and band structures are determined for CdSe, CdS, and ZnS. These band structures are then used to analyze the optical data for these crystals. The calculation confirms some earlier identifications of the optical structure in some cases, and causes new interpretations in other cases. In addition, some previously unidentified structure is explained. A calculation of the imaginary part of the dielectric function is given for hexagonal CdSe and ZnS.

I. INTRODUCTION

THE empirical pseudopotential method[1] (EPM) and related methods have been shown to yield accurate band structures for semiconductors,[2] insulators,[3] semimetals,[4] and metals.[5] With this method, the potential used in the secular equation to find the one-electron energy levels and wave functions is determined by a small number of parameters, the pseudopotential form factors. These parameters are obtained from experimental optical data: In the present work, reflectivity taken over a wide range of energy. The potential is appropriate for the states of interest, the valence and conduction band states, and the core states are not solutions of the secular equation.[6] The present work is a straightforward extension of the work of CB to the hexagonal, wurtzite structure semiconductors ZnS, CdS, and CdSe. The pseudopotential form factors obtained for cubic ZnS (zinc blende) in CB are taken over and are used for the calculation of the band structure of hexagonal ZnS (wurtzite). The knowledge gained in the ZnS calculation aids in the calculation of the band structures of hexagonal CdS and CdSe, using the

† Supported by the National Science Foundation.
* Present address: James Franck Institute, University of Chicago, Chicago, Illinois.
‡ Alfred P. Sloan Foundation Fellow.
[1] M. L. Cohen and T. K. Bergstresser, Phys. Rev. **141**, 789 (1966) (referred to as CB).
[2] Reference 1 and references therein. Also P. M. Lee, Phys. Rev. **135**, A1110 (1964); W. Saslow, T. K. Bergstresser and M. L. Cohen, Phys. Rev. Letters **16**, 354 (1966).
[3] M. L. Cohen, P. J. Lin, D. M. Roessler, and W. C. Walker, Phys. Rev. **155**, 992 (1967).
[4] L. M. Falicov and P. J. Lin, Phys. Rev. **141**, 562 (1966); P. J. Lin and L. M. Falicov, *ibid.* **142**, 441 (1966); P. J. Lin and J. C. Phillips, *ibid.* **147**, 469 (1966).
[5] See, for example, W. A. Harrison, in *Pseudopotentials in the Theory of Metals* (W. A. Benjamin, Inc., New York, 1966).
[6] L. Kleinman and J. C. Phillips, Phys. Rev. **118**, 1153 (1960); M. H. Cohen and V. Heine, *ibid.* **122**, 1821 (1961); B. J. Austin, V. Heine, and L. J. Sham, *ibid.* **127**, 276 (1962).

optical data for these crystals without the form factors having been determined for the corresponding cubic materials.

A calculation of the energy levels of hexagonal ZnS has been made using the orthogonalized plane-wave (OPW) method[7] and the augmented plane-wave (APW) method.[8] An OPW calculation of the energy levels of CdS has been made,[9] and this same work presents an empirical pseudopotential calculation which differs considerably from the present work. In all of the above calculations, the energy levels were obtained only at a few special points in the zone. A condensed report of the present work on ZnS has been given.[10] Previous interpretation of wide-range reflectivity data of wurtzite-structure compounds have been given by Phillips[11] and by Cardona and Harbeke.[12]

In this paper, we present band structures and pseudopotential form factors for hexagonal ZnS, CdS, and CdSe, and for cubic ZnS. We calculate dipole matrix elements as well as energy levels and use them to calculate ϵ_2, the imaginary part of the dielectric function. The band structures and calculated dielectric functions are compared with the experimentally determined optical structures of these substances. This work confirms some of the previous identifications of optical structure,[11,12,13] presents some new interpretations, and explains previously unidentified structure. This work also permits an examination of the relation between the electronic structures in the zinc blende and wurtzite crystals. The use of the EPM permits the calculation of a complete band structure; that is, a band structure determined over a wide range of energy and at many points in the zone. This is the first identification of the optical structure of wurtzite-structure compounds made on the basis of a complete band structure. The present application further tests the EPM and will be helpful in determining its possibilities and limitations. The success in going from cubic to hexagonal ZnS provides further evidence for the fundamental nature of the form factors obtained by the EPM. Given our interpretation, the agreement between experiment and the band structures is 0.01 Ry near the gap and 0.06 Ry over a range of 1.0 Ry. This is comparable to, but not as good as, the accuracy achieved by CB. Some unanswered questions remain and are discussed. Inasmuch as many past difficulties have often been resolved in favor of the EPM by a reinterpretation of optical data, there is a possibility that nonagreement of our band structures with the data will be resolved by new data or by a new interpretation of existing data, rather than by the realization of a breakdown in the EPM. It is expected that this study will be useful in the continuing investigation of these materials.

II. PRELIMINARY DETAILS

We use the same Hamiltonian as CB, but we must use a different reciprocal lattice and a different structure factor.

$$H=-\frac{\hbar^2}{2m}\nabla^2+V(\mathbf{r}), \tag{1}$$

$$V(\mathbf{r})=\sum_{|\mathbf{G}|\leq G_0}[S^S(\mathbf{G})V_G{}^S+iS^A(\mathbf{G})V_G{}^A]e^{+i\mathbf{G}\cdot\mathbf{r}}. \tag{2}$$

Here m is the free-electron mass, $\mathbf{G}$ is a reciprocal lattice vector, S^S and S^A are the symmetric and antisymmetric structure factors, and V^S and V^A are the symmetric and antisymmetric form factors. The structure and form factors are given by

$$S^S(\mathbf{G})=\frac{1}{n}\sum_j e^{-i\mathbf{G}\cdot\delta_j}; \tag{3a}$$

$$S^A(\mathbf{G})=-\frac{i}{n}\sum_j P_j e^{-i\mathbf{G}\cdot\delta_j}, \tag{3b}$$

$$V_G{}^S=\frac{n}{\Omega}\int\tfrac{1}{2}[v^1(\mathbf{r})+v^2(\mathbf{r})]e^{-i\mathbf{G}\cdot\mathbf{r}}d^3r; \tag{4a}$$

$$V_G{}^A=\frac{n}{\Omega}\int\tfrac{1}{2}[v^1(\mathbf{r})-v^2(\mathbf{r})]e^{-i\mathbf{G}\cdot\mathbf{r}}d^3r, \tag{4b}$$

where n is the number of atoms per unit cell (2 for zinc blende and 4 for wurtzite), Ω is the volume of the unit cell, $\boldsymbol{\delta}_j$ is the position vector of the jth atom in the unit cell and the index j includes all the atoms of a unit cell in the summation, P_j is $+1$ if j denotes one type of atom and P_j is -1 if j denotes the other type of atom, and $v^1(\mathbf{r})$ and $v^2(\mathbf{r})$ refer to the potentials of the atoms of type 1 and type 2, respectively. The statement of Eq. (2) and the lack of an angular dependence of the form factors presupposes that the atomic potentials are spherically symmetric, which we assume is a good approximation for our purposes. We make the approximation that the form factors are independent of energy and momentum and that the sum in Eq. (2) may be cut off at an appropriate value G_0. If the center of the unit cell is chosen so that the position of each atom of the first type goes into the position of an atom of the second type upon spatial inversion, then both S^S and S^A are real. This can be done for both zinc blende and wurtzite. Notice that the normalization of the form factors to the volume per atom means that we may use

[7] F. Herman and S. Skillman, in *Proceedings of the International Conference on Semiconductor Physics, Prague, 1960* (Academic Press Inc., New York, 1961), p. 25.
[8] U. Rössler and M. Lietz, Phys. Status Solidi **17**, 597 (1966).
[9] T. C. Collins, R. N. Euwema, and J. S. DeWitt, in *Proceedings of the International Conference on the Physics of Semiconductors, Kyoto, 1966* (The Physical Society of Japan, Tokyo, 1966), p. 15.
[10] T. K. Bergstresser and M. L. Cohen, Phys. Letters **23**, 8 (1966).
[11] J. C. Phillips, Phys. Rev. **133**, A452 (1964).
[12] M. Cardona and G. Harbeke, Phys. Rev. **137**, A1467 (1965); also, in *Proceedings of the International Conference on the Physics of Semiconductors, Paris* (Dunod Cie, Paris, 1964), p. 217.
[13] Many references are devoted to the fundamental band gap. See for example, the references in Table I.

TABLE I. Lattice constants in angstroms, and the parameters of the fundamental gap, in eV. Column 4 contains the intrinsic fundamental gap at low temperature, adjusted to remove the effect of spin-orbit splitting: $\Gamma_6 \rightarrow \Gamma_1$, or for zinc blende, $\Gamma_{15} \rightarrow \Gamma_{15}$. Column 5 contains the parameter δ of the quasicubic model,[a] identified with the spin-orbit splitting. Column 6 contains the parameter α, identified with the crystal-field splitting $\Gamma_1^v \rightarrow \Gamma_6^v$.

	a	c/a	Gap	δ(S.O.)	α(C.F.)	Ref.
ZnS (hex)	3.811	1.636	3.94	0.09	+0.05	b
CdS (hex)	4.136	1.623	2.58	0.06	+0.03	c
CdSe (hex)	4.30	1.633	1.98	0.42	+0.04	d
ZnS (cubic)	5.41		3.84	0.07		e

[a] Reference 18, main text.
[b] W. W. Piper, P. D. Johnson, and D. T. F. Marple, J. Phys. Chem. Solids **8**, 457 (1959), and R. G. Wheeler and J. C. Miklosz, in *Proceedings of the International Conference on Physics of Semiconductors, Paris* (Dunod Cie, Paris, 1964), p. 873.
[c] D. G. Thomas and J. J. Hopfield, Phys. Rev. **116**, 573 (1959).
[d] J. O. Dimmock and R. G. Wheeler, Phys. Rev. **125**, 1805 (1962).
[e] J. L. Birman, H. Samelson, and A. Lempiki, Gen. Tel. Electron. Res. Develop. J. **1**, 2 (1961), as reported in the reviwe of D. C. Reynolds, C. W. Litton, and T. C. Collins, Phys. Satus Solidi **9**, 645 (1965), and by S. L. Adler, Phys. Rev. **126**, 118 (1962). An exciton binding energy of 0.04 eV has been assumed.

zinc blende form factors in wurtzite without a change in normalization. The slight density change on going from zinc blende to wurtzite causes too small a change in form factors to concern us here.

The wurtzite and zinc blende crystal structures are discussed by Wyckoff.[14] See Table I for the lattice parameters used here. Birman[15] discusses the similarity between the two structures in placement of nearest and next nearest neighbors. When the nearest-neighbor distance in the basal plane of wurtzite is the same as the nearest-neighbor distance of zinc blende, the lattice constants are related by $a_{ZB}=\sqrt{2}a_W$. In zinc blende, reciprocal lengths are measured in units of $(2\pi/a_{ZB})$ so that the reciprocal lattice vectors have the smallest possible integers as their Cartesian components. To compare these with the reciprocal lattice vectors of wurtzite, we must measure reciprocal lengths in wurtzite in units of $(\sqrt{2}\pi/a_W)$. Table II shows square magnitudes for the reciprocal lattice vectors of wurtzite and of zinc blende. The magnitudes of the structure factors are also shown in Table II.

We use the symmetry classification of Rashba.[16] Other symmetry classifications differ on the Δ axis and/or the U axis. The biggest pitfall to be observed is that Rashba's Γ_6 is named Γ_5 by some references, and vice versa. For convenience, the selection rules are presented in Table III. The naming of points, lines and planes in the Brillouin zone is shown in Fig. 1.

The cutoff energies in CB were $E_1=7$ and $E_2=19$, giving convergence to <0.1 eV for the group IV elements and the III–V compounds. We find that more plane waves are needed to obtain good convergence for the II–VI compounds because of their large antisymmetric potential. We use $E_1=10$, $E_2=27$ for both zinc blende and wurtzite. At a few places in the zone of wurtzite, we increase E_1 to 10.3. These limits cause a convergence error of <0.1 eV. For wurtzite these limits mean that usually 65–67 plane waves form the basis, with the contribution from about 220 more plane waves being added by the perturbation theory. This large number of plane waves comes about because the wurtzite lattice has as many atoms per unit volume but twice as large a unit cell as the zinc blende lattice, which means that a given volume of reciprocal space contains about twice as many reciprocal lattice points for wurtzite.

We have computed the EPM eigenvalues and eigenvectors on a mesh of 125 points in 1/24 of the Brillouin zone in order to calculate ϵ_2, the imaginary part of the dielectric function, in a manner similar to Brust.[17] We have

$$\epsilon_2^{\parallel}(\omega)=\frac{e^2\hbar^2}{\pi m^2\omega^2}\sum_{c,v}\int_{\mathrm{BZ}}\delta(E_c(\mathbf{k})-E_v(\mathbf{k})-\hbar\omega)\times|\langle u_{\mathbf{k},v}|\frac{d}{dz}|u_{\mathbf{k},c}\rangle|^2 d^3k, \quad (5)$$

where $u_{\mathbf{k},v}$ and $u_{\mathbf{k},c}$ are the periodic parts of the valence and conduction band wave functions. The superscript of ϵ refers to the polarization of the electric vector with respect to the c axis, taken to be in the z direction. For perpendicular polarization, one uses either d/dx or d/dy in the matrix element. It is necessary to use k-dependent matrix elements even when computing an "unpolarized" ϵ, since matrix elements can vary rapidly in k space because of crossing or virtual crossing of bands. Between the mesh points, the bands and matrix elements are approximated by a linear interpolation formula in order to compute the integral in Eq. (5). The mesh is quite coarse, but computing at a larger number of points in the Brillouin zone was felt to be out of the question at this time. The mesh is adequate to show the gross structure, but fine structure is washed out and the peaks are broadened and possibly distorted. The calculated ϵ_2 is adequate to identify the origin in the zone of the major optical structure.

III. THE DATA CONSULTED

This section tabulates the data consulted during the course of this work. It should not be regarded as a compilation of data.

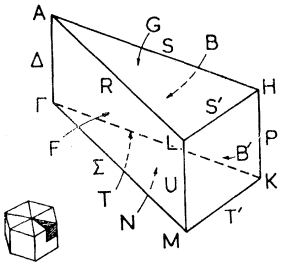

FIG. 1. The hexagonal Brillouin zone of wurtzite.

[14] R. W. G. Wyckoff, *Crystal Structures* (Interscience Publishers, Inc., New York, 1963), Vol. I, pp. 108, 111.
[15] J. L. Birman, Phys. Rev. **115**, 1493 (1959).
[16] E. I. Rashba, Fiz. Tverd. Tela **1**, 407 (1959) [English transl.: Soviet Phys.—Solid State **1**, 368 (1959)].
[17] D. Brust, Phys. Rev. **134**, A1337 (1964).

TABLE II. Reciprocal lattice vectors and structure factors for wurtzite and zinc blende, and form factors, in Ry, used in this work. Column 1 contains a representative from each set of equivalent reciprocal lattice vectors. For zinc blende, these vectors are expressed with respect to a Cartesian coordinate system, but for wurtzite, these vectors are expressed with respect to the primitive translation vectors, the first two of which make an angle of 120°. Column 2 contains the magnitudes of these vectors, and in wurtzite for the case that $c/a=\frac{2}{3}\sqrt{6}=1.633$. Columns 4 and 5 contain the structure factor, and in wurtzite for the case that $u=\frac{3}{8}$. The structure factors which do depend on the crystal structure parameter u are shown as two-place decimal fractions. The remaining columns contain the symmetric and antisymmetric form factors for ZnS, Cds, and CdSe. The form factors for the wurtzite lattice are obtained from the form factors for the zinc blende lattice by interpolation.

G	G^2	$\lvert S^S(\mathbf{G})\rvert$	$\lvert S^A(\mathbf{G})\rvert$	ZnS V^S	ZnS V^A	CdS V^S	CdS V^A	CdSe V^S	CdSe V^A
(Wurtzite)									
000	0	1	0						
001	$\frac{3}{4}$	0	0						
100	$2\frac{2}{3}$	$\frac{1}{2}$	0	−0.24		−0.26		−0.25	
002	3	0.71	0.71	−0.22	0.23	−0.24	0.23	−0.23	0.19
101	3-5/12	0.33	0.80	−0.19	0.19	−0.20	0.18	−0.20	0.15
102	$5\frac{2}{3}$	0.35	0.35	−0.06	0.10	−0.03	0.08	−0.07	0.09
003	$6\frac{3}{4}$	0	0						
210	8	1	0	+0.03		+0.03		+0.01	
211	$8\frac{3}{4}$	0	0						
103	9-5/12	0.80	0.33	+0.06	0.03	+0.04	0.05	+0.03	0.05
200	$10\frac{2}{3}$	$\frac{1}{2}$	0	+0.07		+0.04		+0.04	
212	11	0.71	0.71	+0.07	0.02	+0.04	0.05	+0.04	0.05
201	11-5/12	0.33	0.80	+0.07	0.02	+0.04	0.05	+0.04	0.05
004	12	0.00	1.00		0.02		0.05		0.05
202	$13\frac{2}{3}$	0.35	0.35	+0.04	0.01	+0.02	0.03	+0.02	0.03
104	$14\frac{2}{3}$	0.00	0.50		0.01		0.02		0.02
213	$14\frac{3}{4}$	0	0						
(Zinc blende)									
000	0	1	0						
111	3	$\frac{1}{2}\sqrt{2}$	$\frac{1}{2}\sqrt{2}$	−0.22	0.23	−0.24	0.23	−0.23	0.19
200	4	0	1		0.15		0.13		0.12
220	8	1	0	+0.03		+0.03		+0.01	
311	11	$\frac{1}{2}\sqrt{2}$	$\frac{1}{2}\sqrt{2}$	+0.07	0.02	+0.04	0.05	+0.04	0.05
222	12	0	1		0.02		0.05		0.05
400	16	1	0	0		0		0	

The region of the fundamental gap has been extensively studied and is well understood. This work does not attempt to attain the accuracy of these studies; we are mainly interested in the energy of the intrinsic gap to within $\frac{1}{10}$ eV. The preparation of Table I has involved the use of the limits or estimated limits of the free exciton series to calculate the parameters α and δ of the quasicubic model.[18] The parameter α is taken to be the crystal field splitting of the valence band, $\Gamma_1^v \rightarrow \Gamma_6^v$. The splitting in energy of the fundamental gap without spin-orbit coupling, $\Gamma_6^v \rightarrow \Gamma_1^c$, is $E_a+\frac{1}{3}\delta$, where E_a is the value of the gap with spin-orbit coupling, $\Gamma_9^v \rightarrow \Gamma_7^c$, and δ is the spin-orbit coupling parameter. This neglects interaction of the top of the valence band with other bands via spin-orbit coupling, which is too small an effect for our purposes. The parameters of cubic ZnS are also summarized in Table I.

The bulk of the experimental information comes from reflectivity measurements taken over a wide range of energy. Reflectivity spectra have been taken of cubic ZnS;[12,19,20] and hexagonal ZnS with polarized light,[21] also at low temperature,[21] and with light of mixed polarization.[20,22] ("Mixed" denotes approximately unpolarized light.) Reflectivity spectra have been taken of cubic CdS;[23] and hexagonal CdS with polarized light,[12,21,24] with $\perp$ and mixed polarization,[20] and with mixed polarization.[22,25] Reflectivity spectra have been taken of hexagonal CdSe with polarized light,[12,21] and mixed

TABLE III. Selection rules for wurtzite. Dipole transitions from a state listed on the left of a double arrow to a state on the right of a double arrow, and vice versa, are allowed. For $E\|c$ only transitions between states of the same symmetry are allowed.

$E\perp c$

$\Delta_1, \Delta_2, \Delta_5 \leftrightarrows \Delta_6$

$\Delta_3, \Delta_4, \Delta_6 \leftrightarrows \Delta_5$

$U_1, U_4 \leftrightarrows U_2, U_3$

$P_1, P_2, P_3 \leftrightarrows P_3$

$E\|c$

$X_i \leftrightarrows X_i$

[18] J. J. Hopfield, J. Phys. Chem. Solids **15**, 97 (1960); S. L. Adler, Phys. Rev. **126**, 118 (1962).

[19] W. C. Walker and J. Osantowski, J. Opt. Soc. Am. **53**, 399 (1963); and (private communication).

[20] M. Balkanski and Y. Petroff, in *Proceedings of the International Conference on the Physics of Semiconductors, Paris* (Dunod Cie, Paris, 1964), p. 245.

[21] M. Cardona, Solid State Commun. **1**, 109 (1963).

[22] M. Cardona, Phys. Rev. **129**, 1068 (1963).

[23] M. Cardona, M. Weinstein, and G. A. Wolff, Phys. Rev. **140**, A633 (1965).

[24] W. C. Walker, Phys. Rev. Letters **13**, 51 (1964).

[25] W. C. Walker and J. Osantowski, J. Phys. Chem. Solids **25**, 778 (1964).

polarization.[20,22,26] Kramers-Kronig inversions have been made of some of the spectra of Refs. 12, 20, 23, 26, and 27. The energies of peaks of the various references usually agree rather closely, with exceptions to be noted in Secs. IV and V. However, the relative sizes of peaks agree less well; exceptions to agreement are also noted in these sections. The results of our calculations should be compared to the imaginary part of the dielectric function, $\epsilon_2(\omega)$ but since the various sources are not always in agreement as to the shift in peak energy caused by the transformation from reflectivity, R to ϵ_2, and since the structure of R is quite similar to the structure of ϵ_2, we will make our discussions with respect to the reflectivity, with occasional reference to ϵ_2.

There is no convenient nomenclature for the peaks. We will use the notation of Cardona and Harbeke,[12] but without the implications that this notation has regarding the origin in the Brillouin zone of the peaks. Table IV summarizes the experimental reflectivity peak energies which we use in this work.

Other types of data may be brought to bear on the problem of determining the band structure of these substances although they are not as extensive as reflectivity. The photoemissive yields and distributions have been studied for CdS[28] and CdSe,[29] and in addition electroreflectance experiments have been done on these crystals.[30,31]

IV. ZnS

The pseudopotential form factors of ZnS have previously been found in CB. Each symmetric form factor was required to be the average of the corresponding form factors of Si and Ge. The antisymmetric form factors were determined by requiring them to result in a band structure that is consistent with the reflectivity data of cubic ZnS. We emphasize that only three parameters; i.e., three antisymmetric form factors, are determined from the optical data of cubic ZnS in order to compute its band structure. The antisymmetric form factors used here have been redetermined from the same data and are slightly different. The old form factors included the effects of a slight nonconvergence (~0.1 eV). Also, here we require $V_{11}^A = V_{12}^A$ (instead of $V_{12}^A = 0$) so that a smooth curve for V^A as a function of K^2 may be drawn.[32] We use these form factors to compute the band structure of hexagonal ZnS. The form factors need to be interpolated since the magnitudes of the reciprocal lattice vectors in wurtzite are in general not the same as those in zinc blende. The interpolation is straightforward since the reciprocal lattice vectors in wurtzite whose magnitudes are not close to a zinc-blende value have either a zero or a small structure factor, with the exception of number 10 in Table II. Thus, the optical spectrum of zinc blende generates the band structure of wurtzite. This use of interpolation has the character of an analytic continuation of the empirical form factors.[33] The form factors used here for cubic ZnS and the interpolated values for hexagonal ZnS are given in Table II. We continue the practice of requiring that a form factor be expressed as an integer number of hundredths of a Rydberg.

Figure 2 shows the calculated band structure for hexagonal ZnS; Fig. 3 shows that for cubic ZnS. The conduction and valence band edges are at the center of the zone in both structures,[34] so that both are direct gap materials. The general features of the calculated zinc blende band structure have been discussed in CB,

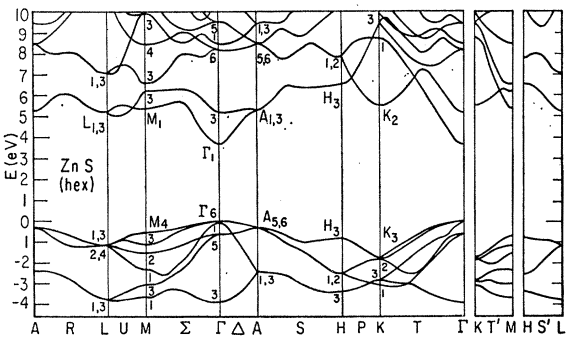

FIG. 2. Band structure of hexagonal ZnS.

TABLE IV. Position in energy of peaks in reflectivity (eV). For the E_1 peaks, we give low-temperature values; other values are room-temperature values and are not expected to shift by more than 0.1 eV upon going to low temperature.

	ZnS cubic	ZnS $E\perp c$	ZnS $E\parallel c$	CdS $E\perp c$	CdS $E\parallel c$	CdSe $E\perp c$	CdSe $E\parallel c$
E_1A				5.0[c]		4.3[c]	
E_1B	5.9[a]	5.75[a]	5.75[a]	5.6	5.7	4.9	5.0
E_0'				6.2[b]	6.3[b]		6.1[b]
F_1		6.6[b]		7.1		6.8	
E_2	7.0/7.4	7.0/7.5[b]	7.0/7.5	8.0[d]	8.0[d]	7.5	7.5
E_1'	9.8	9.6	9.7	9.2	9.3	8.4	8.6
F_3[b]				9.8	9.8	9.2	9.3

[a] The E_1 peak of ZnS is not split into part A and part B. This peak is named E_0' in Ref. 12, main text.
[b] Shoulder.
[c] Average of spin-orbit split peaks.
[d] This peak has a weak shoulder 0.4 eV higher.

[26] J. S. DeWitt, thesis, Air Force Institute of Technology, 1965 (unpublished).
[27] A. Kramers-Kronig inversion for hex. CdS, mixed polarization, has been provided by W. C. Walker (private communication).
[28] N. B. Kindig and W. E. Spicer, Phys. Rev. 138, A561 (1965).
[29] J. L. Shay (unpublished).
[30] M. Cardona, K. L. Shaklee, and F. H. Pollak, Phys. Rev. 154, 696 (1967).
[31] F. Oluwole and Y. R. Shen (private communication).

[32] Either way we get the same number of parameters to be determined. For the III–V compounds it makes little difference which prescription we choose since the form factors are small in this region of K^2. In any case, one gets virtually the same band structure with $V_{11}^A = X$, $V_{12}^A = 0$; or with $V_{11}^A = \frac{1}{2}X$, $V_{12}^A = \frac{1}{2}X$.
[33] J. C. Phillips, in *Proceedings of the International Conference on the Physics of Semiconductors, Kyoto, 1966* (The Physical Society of Japan, Tokyo, 1966), p. 3.
[34] The spin-orbit coupling will cause the valence band edge to lie a very small distance away from Γ, but this is too fine an effect to concern us here. See, for example, G. D. Mahan and J. J. Hopfield, Phys. Rev. 135, A428 (1964).

TABLE V. The change, in eV, of the difference between energy levels for a change in form factor of +0.01 Ry. Symmetric and antisymmetric form factors for hexagonal ZnS and antisymmetric form factors for cubic ZnS are tabulated.

G^2	$\Gamma_6 \to \Gamma_1$	$\Gamma_1^v \to \Gamma_6^v$	$\Gamma_5 \to \Gamma_3$	$\Gamma_5 \to \Gamma_6$	$\Gamma_1 \to \Gamma_1$	$M_4 \to M_3$	$M_3^v \to M_4^v$	$M_2 \to M_1$	$H_3 \to H_3$	$K_3 \to K_2$	$K_2^v \to K_3^v$
						V^S					
$2\frac{2}{3}$	−0.08	−0.05	−0.05	−0.09	−0.07	−0.07	−0.05	−0.10	−0.04	−0.17	+0.09
3	−0.08	+0.10	−0.03	−0.02	+0.01	−0.05	+0.12	−0.03	−0.07	−0.04	−0.12
3-5/12	−0.02	−0.07	−0.07	−0.03	−0.11	−0.04	−0.05	−0.06	−0.08	−0.06	+0.06
$5\frac{2}{3}$	−0.02	+0.07	−0.05	−0.03	−0.02	−0.08	+0.07	−0.03	−0.01	+0.05	−0.04
8	+0.20	−0.29	+0.21	−0.07	−0.12	+0.10	−0.25	+0.10	−0.12	−0.21	+0.24
9-5/12	−0.05	+0.37	−0.14	−0.08	−0.06	−0.05	+0.31	−0.08	+0.21	+0.19	−0.31
$10\frac{2}{3}$	+0.08	−0.08	+0.10	+0.07	−0.03	+0.07	−0.07	+0.04	−0.03	−0.01	+0.04
11	+0.17	+0.01	+0.06	−0.02	+0.02	+0.09	−0.04	+0.02	+0.08	+0.07	+0.02
11-5/12	+0.03	+0.06	+0.03	−0.01	−0.04	+0.02	−0.04	+0.01	−0.03	−0.04	+0.03
$13\frac{2}{3}$	+0.06	−0.03	+0.05	+0.02	0.00	+0.07	−0.03	+0.02	+0.02	+0.01	+0.01
						V^A					
3	+0.05	−0.07	−0.02	+0.02	0.00	+0.04	−0.09	+0.01	+0.02	+0.04	+0.08
3-5/12	+0.19	−0.08	+0.31	+0.31	+0.32	+0.22	+0.05	+0.28	+0.23	+0.25	−0.09
$5\frac{2}{3}$	0.00	−0.03	+0.03	+0.04	+0.07	+0.03	−0.04	+0.02	+0.02	−0.03	+0.03
9-5/12	−0.01	−0.07	+0.01	+0.02	−0.04	0.00	−0.07	+0.01	−0.04	−0.03	+0.06
11	−0.16	+0.08	−0.05	0.00	+0.12	−0.08	+0.07	−0.01	−0.05	−0.01	−0.06
11-5/12	−0.27	+0.19	−0.24	−0.14	+0.02	−0.12	+0.15	−0.11	+0.01	+0.08	−0.15
12	−0.01	−0.14	0.00	+0.01	−0.18	0.00	−0.11	0.00	−0.08	−0.05	+0.11
$13\frac{2}{3}$	−0.06	+0.03	−0.03	−0.03	0.00	−0.03	+0.02	−0.01	−0.03	+0.01	−0.02
$14\frac{2}{3}$	−0.03	−0.11	+0.01	+0.01	−0.10	0.00	−0.09	0.00	−0.09	−0.07	+0.09

G^2	$\Gamma_{15} \to \Gamma_1$	$L_3 \to L_1$	$\Gamma_{15} \to \Gamma_{15}$	$L_3 \to L_3$	$X_5 \to X_1$
			V^A		
3	+0.12	+0.08	+0.14	+0.16	+0.22
4	+0.14	+0.26	+0.28	+0.17	+0.04
11	−0.29	−0.15	+0.04	−0.03	−0.11
12	−0.22	−0.15	−0.18	−0.02	0.00

so that the following comments concentrate on wurtzite. The calculations show the conduction band edge very definitely to be at Γ. The next edge, also at Γ, is 2 eV higher. Below the valence band edge at Γ are edges at M and H. The calculation of Herman and Skillman[7] found the top of the valence band to lie at M with lower edges at H and at Γ. In spite of differences in detail, this work shows an over-all similarity with ours.

Let us concentrate our attention on the similarity in Figs. 2 and 3 of the cubic and the hexagonal band structure. The work of Birman[15] using tight-binding wave functions shows that there is a correspondence between states along the Λ symmetry line (cubic) and states along the Δ symmetry line going from Γ to A and back to Γ (hexagonal). One reason is the similarity of the Brillouin zones when aligned as done by Birman. The two zones are aligned so that one of the cubic Λ axes lies along the hexagonal Δ axis. In this case, the hexagonal planes of the two direct lattices are parallel. Figure 4 shows the aligned zones and also shows where special points of the cubic zone lie in the hexagonal zone. In addition to the zone similarity, the matrices of the tight-binding calculation using s and p orbitals on the atomic sites are similar. The first reason for similarity applies to our EPM calculation; the second reason applies insofar as the EPM wave functions along this symmetry line are expressable as s and p tight-binding functions. The Birman correspondence yields the result: Γ_1, L_1, and L_3 (cubic) correspond to Γ_1, Γ_3, and Γ_5, (hexagonal) respectively; Γ_{15} (cubic) corresponds to Γ_6 plus Γ_1 (hexagonal), using the Rashba[16] symmetry notation.

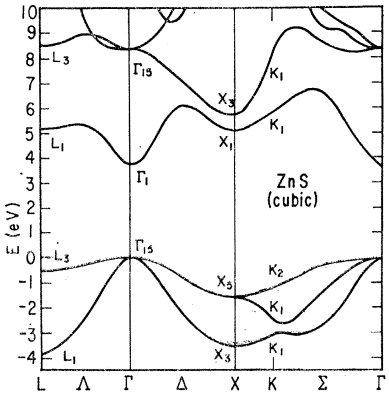

FIG. 3. Band structure of cubic ZnS.

The energy difference between corresponding levels is seen to be surprisingly small in our calculations. Those wurtzite levels below and including the second Γ_1 in the conduction band lie within 0.2 eV of their corresponding zinc blende levels. The Γ_5 level in the conduction band lies 1 eV higher than the corresponding zinc blende level. Notice also the similarity between the Λ direction in zinc blende and the "unfolded" Δ direction in wurtzite. As noted before, the form factors were not chosen to give any particular result in the wurtzite band structure, but are the result of an extrapolation of the zinc blende form factors. The obtaining of such a correspondence need not necessarily hold.

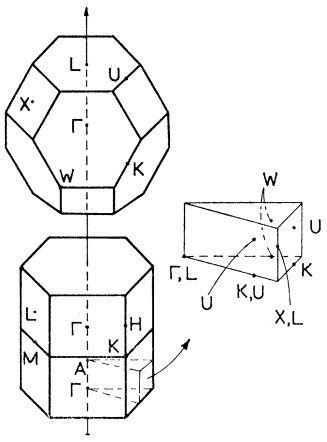

FIG. 4. Comparison of zones: Aligned zones of zinc blende and wurtzite, and positions in the hexagonal zone of special points of the cubic zone.

One can see this using the derivatives of the energy levels with respect to the form factors, Table V. For example, in the cubic case, V_3^A and V_4^A affect the bands considerably, although their effects are somewhat similar, while in the hexagonal case in this region of magnitude of the wave vector, only V^A ($G^2=2\frac{2}{3}$) has a strong influence. Also, the crystal-field splitting at Γ in the valence band would not be correct for many choices of form factors. If the band structure of a hypothetical substance which has all the parameters of ZnS except a zero antisymmetric potential is computed, we find that the corresponding levels are still rather close in energy; the deviations are not more than $\frac{1}{2}$ eV except for the Γ_5 level in the conduction band. Apparently, the similarity of the two zones involved is quite influential.

The similarity of optical structure between wurtzite and zinc blende holds for more than the structure arising from states near the Δ axis of wurtzite. When the two zones are aligned as in Fig. 4, the correspondence of a cubic Λ axis with the hexagonal Δ axis is unambiguous. The correspondence of other parts of the zones is not unambiguous.[15] Nonetheless, the correspondences actually found in our calculations are generally indicated by the mapping of cubic zone points into the hexagonal zone as shown in Fig. 4. This is discussed further in the following paragraphs.

Our task now is to examine the calculated band structure of wurtzite in detail, and to explain the observed optical data on the basis of our band structure. Table VI summarizes the splittings of energy levels to be discussed, along with their associated structure in the calculated ϵ_2. The experimental reflectivity peaks which we conclude are caused by the structure in ϵ_2 are also given. The calculated ϵ_2 for wurtzite is presented in Fig. 5. We have examined the separate contribution to ϵ_2 of the individual pairs of bands and of the various regions of the zone. Because of the large number of bands and of distinct regions in the zone, it is impractical to present the separate parts of ϵ_2 in graphical form. We present below the results of examining the separate contributions.

The fundamental gap is well understood and is attributed to $(\Gamma_6,\Gamma_1)\rightarrow\Gamma_1$ transition in wurtzite and to $\Gamma_{15}\rightarrow\Gamma_1$ transitions in zinc blende. Spin-orbit coupling slightly modifies the optical structure here. Our band structures are satisfactory with respect to these transitions.

In the cubic materials, the first major peak in ϵ_2, called E_1 or the Λ peak, comes from transitions in the region of an M_1 critical point (cp) lying on the Λ axis.[17,35,36] For Ge, Sn, and the III–V compounds, this cp lies about 0.4 of the way from Γ to L, but in the II–VI compounds this cp lies very close to L: 0.8 or 0.9 of the way from Γ to L. In this case the interband energy at the M_1 cp

TABLE VI. Identification of optical structure of hexagonal ZnS. Column 1 lists the important regions of the zone and Column 2 lists the important transitions in these regions. Column 3 lists the energy and Column 4 lists the square of the magnitude of the dipole matrix element in relative units of the transition in Column 2. The squares of the matrix elements are summed over initial and/or final states in the case of degeneracy. Column 5 lists the energy of structure in the calculated $\epsilon_2(\omega)$ caused by the region listed in Column 1. Shifts of $\sim$0.2 eV or more may be expected because of the coarse mesh used to calculate ϵ_2. The last column names the reflectivity structure caused by the regions and transitions listed.

Region	Trans.	eV	ME	ϵ_2	Ident.
M_0 cp at	$\Gamma_6\rightarrow\Gamma_1$	3.8	1.4 $\perp$	3.8	Gap
M_0 cp at	$\Gamma_1\rightarrow\Gamma_1$	3.8	1.4 $\parallel$	3.8	Gap
M_1 cp near	$\Gamma_5\rightarrow\Gamma_3$	5.8	1.8 $\perp$	6.0	E_1
M_1 cp near	$U_4\rightarrow U_3$	5.9	0.7 $\perp$	6.0	E_1
M_1 cp near	$U_3\rightarrow U_3$	5.9	1.0 $\parallel$	6.1	E_1
Region around	$M_2\rightarrow M_1$	6.9	1.5 $\perp$	6.7 and 6.9	F_1 and F_2
Region around	$K_3\rightarrow K_2$	7.3	0.8 $\perp$	7.2	E_2
Large region including	$H_3\rightarrow H_3$	7.4	2.3 $\parallel$	7.0 and 7.4	E_2
Region around	$K_2\rightarrow K_2$	7.5	1.4 $\parallel$	7.4	E_2
Large region including	$\Gamma_5\rightarrow\Gamma_6$	8.9	2.6 $\perp$	8.7	E_1'
Very large region	$\Gamma_1\rightarrow\Gamma_1$	8.6	2.1 $\parallel$	8.5 and 9.0	E_1'

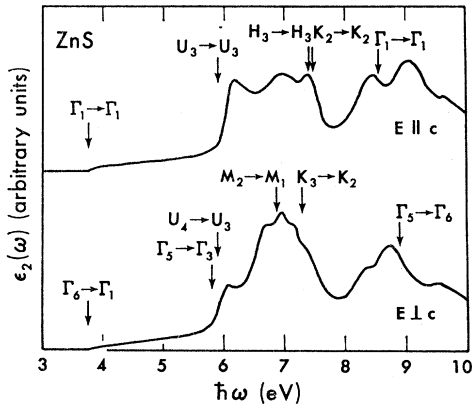

FIG. 5. Computed $\epsilon_2(\omega)$ in arbitrary units as a function of ω in eV for hexagonal ZnS.

[35] T. K. Bergstresser, M. L. Cohen, and E. W. Williams, Phys. Rev. Letters 15, 662 (1965).

[36] W. Saslow, T. K. Bergstresser, C. Y. Fong, M. L. Cohen, and D. Brust, Solid State Commun. 5, 667 (1967).

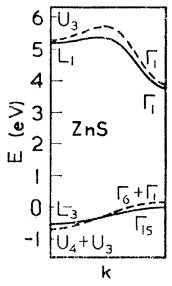

FIG. 6. Comparison of the energy levels along the Λ axis in zinc blende with the levels along a corresponding line in wurtzite. The line in wurtzite begins at Γ and ends on the U axis $\frac{2}{3}$ of the way from M to L. The bands of wurtzite are indicated by broken lines. The two valence bands of wurtzite are practically degenerate.

is within a few hundredths of an electron volt of the interband energy at the M_0 cp lying precisely at L. The net effect is that of an M_1 cp lying at L. We find this cp to have an interband energy of 5.7 eV in zinc blende, and this is to be compared with the E_1 reflectivity peak at 5.9 eV.

For wurtzite the first large peak in reflectivity is also the E_1 peak at about 5.75 eV for both polarizations. (We do not accept the assignment of this peak by Ref. 12 in which it is labeled E_0'.) Such a peak is seen in our calculations of ϵ_2. This calculated peak is similar in appearance to the calculated Λ peak for Ge,[17] and GaAs,[36] and it bears a satisfactory relation to the E_1 peak of reflectivity. The coarse mesh used for ϵ_2 makes these peaks appear $\sim$0.2 eV higher than they would with a fine mesh. A fraction of the peak for $\perp$ polarization comes from transitions in the region of the Δ axis near Γ centered about the transition $\Gamma_5 \rightarrow \Gamma_3$. We find an M_0 cp at Γ with an energy of 5.8 eV. At the same energy is an M_1 cp lying about half-way between Γ and A. This is just what one would expect from the correspondence discussed previously.

The rest of the peak for $\perp$ polarization comes from a rather small region around the U axis except very near both L and M, involving the transitions $U_4 \rightarrow U_3$. We find an M_0 cp on the U axis 0.6 of the way from M to L with an interband energy of 5.9 eV. We find an associated M_1 cp lying close by, inside the zone, and in the direction of Γ. The peak for $\parallel$ polarization comes from a slightly larger region around the U axis but excluding the immediate vicinity of M, and involving the transition $U_3 \rightarrow U_3$. We again find an M_0 cp on the U axis 0.7 of the way from M to L, and with the same interband energy of 5.9 eV, and also with an associated M_1 cp in the direction of Γ. The negative mass direction of both of the M_1 cp points toward Γ. These transitions have virtually the same energy as those along Δ contributing to the E_1 peak, so that the calculated structure is not a split peak, nor does it exhibit much polarization dependence. This agrees with the experimental data.

With the zones aligned, the point L (cubic) is mapped onto Γ as discussed and also onto the U axis 0.67 of the way from M to L (hex). The preceding paragraph has revealed how very nearly the same are the wurtzite and zinc blende band structure at the corresponding locations in the zones. Also see Fig. 6, where the bands of cubic ZnS along the Λ axis are compared with those of hexagonal ZnS along a line from Γ to U (0.67 of the way from M to L). The similarity is striking. The similarity in band structure causes the optical structure in wurtzite and zinc blende to be nearly the same, as is observed. Not only the interband energies come into play, but also the matrix elements. If transition in wurtzite such as $U_3 \rightarrow U_1$, $\Gamma_6 \rightarrow \Gamma_3$, etc., were strong, they would add extra structure to wurtzite. In fact, they are either forbidden or are extremely weak.

In the reflectivity data there is some structure on the low-energy side of the E_1 peak, seen most clearly at low temperature.[21] The structure is seen for both polarizations but is stronger for $\perp$ polarization. Our band structure shows no evidence for structure here. If this structure is due to either $\Delta_5 \rightarrow \Delta_3$ or $U_4 \rightarrow U_3$ transitions, then the form factors for hexagonal ZnS would have to be modified considerably. In this case, the band structure of cubic ZnS would not be given by these modified form factors. An electroreflectance measurement would be helpful in identifying this structure. Similar structure has been observed in CdS.[37] In this case, it cannot be due to the $\Delta_5 \rightarrow \Delta_3$ or $U_4 \rightarrow U_3$ transitions, since these cause the E_1A and E_1B peaks, respectively. Therefore, there is no band-structure explanation for this peak, even if our band structures need to be modified somewhat. On the basis of our calculated band structures, we conclude that this structure in ZnS and in CdS may not be intrinsic. An exciton explanation is possible but not likely.

In the cubic materials the second major peak in ϵ_2, called E_2 or somewhat deceptively the X peak, comes from a region of the zone which includes an M_1 cp at or near X and an M_2 cp near K.[17,36] The terminology "X peak" is somewhat unfortunate since X lies on the edge rather than in the center of the contributing region,[38] although the X transition "moves with" the peak when form factors are changed. However, in the very ionic substance MgO, it is found[3] that the X transition is more than 1 eV lower than the corresponding peak, and in cubic ZnS it is about $\frac{1}{2}$ eV lower. The X_5-X_1 splitting is 6.6 eV, the splitting at K is 7.1 eV and the M_2 cp on the Σ axis is at 7.3 eV.

In wurtzite the E_2 peak has a shoulder at 6.6 eV for $\perp$ polarization only, labeled F_1. We find such a shoulder in our calculated ϵ_2. It comes from the F face of the zone beginning at the U axis and extending almost half-way toward the Δ axis. The point M is on the edge of this region. Critical points are required by symmetry in wurtzite at M. Between the top four valence states and the first two conduction-band states, we need consider only $M_4 \rightarrow M_3$ and $M_2 \rightarrow M_1$ at 6.7 and 6.9 eV, transitions allowed for $\perp$ polarization. All other transitions at M have either a zero or a small dipole matrix

[37] M. S. Brodin and M. I. Strashnikova, Fiz. Tverd. Tela 8, 684 (1966) [English transl.: Soviet Phys.—Solid State 8, 549 (1966)].
[38] E. O. Kane, Phys. Rev. 146, 558 (1966).

element. By separating out the contribution of the various bands to ϵ_2, we see that it is primarily the states associated with $M_2 \rightarrow M_1$ that cause the F_1 shoulder. The E_2 peak itself arises from transitions in a very large region around M. Contributing to the second part of the E_2 peak are the transitions associated with $K_3 \rightarrow K_2$. Transitions near H, although they have the correct energy, do not contribute to ϵ_2 for $\perp$ polarization because of a small matrix element. The E_2 peak for $\parallel$ polarization comes from a very broad region around H. The regions around K and immediately around the cp at H contribute to the second part of the E_2 peak.

The cubic points X, K, and U (U differs from K by a reciprocal lattice vector) are mapped into several different locations. Figure 4 shows that there are two different regions where these points lie: A region around M and extending along the Σ axis, and a region around K and extending up in the z direction. We have already seen that the F_1 peak comes from transitions in the former region, and that E_2 comes from the latter. Thus the F_1 peak is established as a split-off part of the E_2 peak. With respect to the correspondence to the cubic band structure, we see from the transitions involved in the E_1 and F_1 peaks that the states U_3^v, U_4^v, and U_3^c are L-like states, and U_2^v and U_1^c are X-like states. Transitions between states of the two types are forbidden or have a negligible matrix element. The state U_1^v may not be described in this way. One might suppose that an F_1 peak of $\parallel$ polarization at a higher energy could arise from $U_1 \rightarrow U_1$ transitions, but the matrix element for this is negligible.

For all of the structure so far discussed, the final state is the first or second conduction band. The structure arising from the higher conduction bands begins abruptly at 8 eV. This is evidenced by the big dip at about 8 eV in the calculated ϵ_2 and the dip at 8.7 eV in the experimental reflectivity. After this dip comes the E_1' peak. For $\perp$ polarization, this peak comes from a broad region in the center of the zone which may be characterized by the transition $\Gamma_5 \rightarrow \Gamma_6$.[39] For $\parallel$ polarization, the peak comes from an even broader region in the center of the zone and may be characterized by the transitions $\Gamma_1 \rightarrow \Gamma_1$ (second Γ_1). In cubic ZnS the E_1' peak is due to transitions centered partially at L and characterized by $L_3 \rightarrow L_3$. Our calculated E_1' peaks at about 9 eV are 0.7 eV lower than the E_1' peaks in reflectivity. We must remember that the transformation from R to ϵ_2 will shift the reflection peak downward somewhat, perhaps as much as 0.5 eV. Also, as explained in CB, we expect that the lack of an energy dependence in our form factors causes these calculated higher energy peaks to be lower than they should be. For $\parallel$ polarization the E_1' peak has an unwanted precursor peak at 8.5 eV. This comes from a broad region on the top of the zone centered about L, and involving the transitions $L_3 \rightarrow L_3$ and $L_1 \rightarrow L_1$, where the final states are the third and fourth conduction bands. Either these states should be higher, or the dipole matrix elements for these transitions should be less. We point out that the EPM is not expected to give these matrix elements exactly. We expect an error of $\sim 20\%$.[6] We also expect some error because the perturbation contribution is not added when computing these matrix elements. Thus, matrix elements might cure this problem. The E_1' peak for $\perp$ polarization is also lopsided. The transitions on the low-energy side also come from a region about L involving the transitions $L_3 \rightarrow L_1$ and $L_1 \rightarrow L_3$, but the matrix element is much smaller.

[39] One might expect, on the basis of a straightforward application of the Birman correspondence, that this transition would have a small matrix element and that $\Gamma_6 \rightarrow \Gamma_6$ and $\Gamma_5 \rightarrow \Gamma_5$ would have large matrix elements. Actually it is the other way around. The correspondence need not apply to matrix elements when the existence of a nonzero matrix element depends upon overlap of the tight-binding wave functions.

V. CdS, CdSe

The form factors for CdS and CdSe have not previously been determined. We determine them here using the optical data on the hexagonal materials. The procedure is the same as for the cubic materials. A trial set of form factors at the cubic value of the reciprocal lattice vectors is chosen, interpolated, and used to calculate a hexagonal band structure. This band structure is compared with experiment, and the process is stopped when a satisfactory band structure is found. No attempt is made to take advantage of the large number of individual form factor values in the hexagonal structure. The antisymmetric potentials for both CdS and CdSe are quite strong. This is to be expected since the high-energy reflectivity peaks occur at about the same energy or higher energy than in ZnS, even though the lattice constants for CdS and CdSe are larger. The symmetric form factors have also been adjusted in finding the best band structure. In the previous calculations[1] the symmetric form factors were chosen for the III–V and II–VI compounds in the most simple way. For example, the symmetric form factors of Ge were used in ZnSe. This is an adequate approximation because ZnSe does have nearly the same symmetric potential as Ge. However, it is not adequate in CdS to use the symmetric form factors of Ge because of the strong antisymmetric potential, because of the different sizes of the constituent atoms, and because the nearest neighbor distance is different from that of Ge. Therefore, the symmetric form factors of CdS differ from those of Ge. For CdSe, we use a set of symmetric form factors that are given by the average of the CdS symmetric form factors and those of Sn. The form factors for CdS and CdSe are given in Table II.

The band structure of CdS is presented in Fig. 7, that of CdSe in Fig. 8. They are similar to the band structure of ZnS, Fig. 2. The calculated ϵ_2 for CdSe is presented in Fig. 9. Table VII summarizes the energy-level splittings and reflectivity peaks of CdS and CdSe to be discussed. The band structures are satisfactory

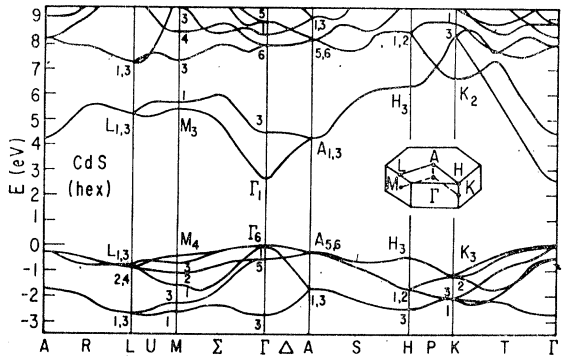

FIG. 7. Band structure of hexagonal CdS.

near the fundamental gap. Spin-orbit coupling modifies the CdSe band structure here to an extent that is noticeable on the scale of Fig. 7.

In CdS and CdSe, the E_1 peak in reflectivity is split into two parts: A and B. Part A is spin-orbit split and is allowed only for $\perp$ polarization.[21] Part B is not observed to be spin-orbit split and lies at about the same energy for both polarizations. The E_1A and E_1B peaks are separated by 0.6 to 0.7 eV. We find that E_1B is caused by the transitions $U_4 \rightarrow U_3$ and $U_3 \rightarrow U_3$, in the same manner as in ZnS. Notice how the levels M_3 and M_1 in the conduction band have changed places compared with ZnS. In these substances it appears that the M_1 cp lies on the U axis for both polarizations. The M_0 cp on the U axis is not resolved as in ZnS. The strong antisymmetric potential makes the M_0 cp insignificant.

We find that the M_1 cp along the Δ axis is at Γ for the same reason as above. For CdS and CdSe, the transition at this cp, $\Gamma_5 \rightarrow \Gamma_3$, has an energy 0.7 eV less than the transitions at the cp along U, whereas in ZnS all the transitions are at about the same energy. In CdS and CdSe, these Γ transitions cause the E_1A peak in reflectivity. The transitions do not show up very well in the calculated ϵ_2 because of the coarse mesh used in this calculation. For parallel polarization, there is no trace of an E_1A peak. In fact, for this polarization, the second conduction band contributes virtually nothing to ϵ_2.

The F_1 peak, allowed for $\perp$ polarization, is seen very well in our calculated ϵ_2, although it is about 0.6 eV lower than the reflectivity peak. For CdS and CdSe, the F_1 peak is an isolated peak rather than a shoulder to the E_2 peak, both in the calculated ϵ_2 and in the reflectivity. This peak comes from the region around M and extending toward Γ, involving the transitions $M_2 \rightarrow M_1$. The contributing region is mostly contained in the lower half of the zone. The transition $M_4 \rightarrow M_3$ makes no contribution here, although it does for ZnS. In fact, these transitions contribute to E_1B. There is an M_2 cp at $M_2 \rightarrow M_1$; the interband energy increases in the direction of K.

Notice that there is some structure in the calculated ϵ_2 for $\parallel$ polarization at about the same energy as the calculated F_1 peak. It is not so much a peak, but rather a sharp dropoff in ϵ_2; it comes from the region around H. There is no F_1 peak in the data for $\parallel$ polarization. Let us analyze the contribution to ϵ_2 for $\parallel$ polarization from the B plane of the zone, considering transitions ending in the first conduction band. We consider only the triangle with corners at Γ, K, and H; the dipole matrix element is small in the other triangle. For now we neglect the K_2 level which comes cutting through the other levels. We denote by E_Γ the splitting at the Γ point, etc. The solid line of Fig. 10 shows schematically the contribution of these transitions to ϵ_2. The contribution from the rest of the zone and the contribution from the transitions terminating near K_2 are added with dotted lines. Figure 10 suggests that E_K is at the energy of the E_2 peak (see next paragraph) and that E_H is at the energy of the E_0' peak in reflectivity. If this is so, then there is only very weak structure for $\perp$ polarization due to H because the matrix elements are small. E_0' in CdSe is indeed observed for $\parallel$ and not for $\perp$ polarization. It is observed for both polarization in CdS, perhaps because of a breakdown in selection rule due to surface condition. Our calculated peak due to H is much stronger than the observed E_0' peak, except for the data of DeWitt[26] in CdSe.

The E_2 peak of CdS and CdSe is much smaller and at much higher energy than for ZnS. This peak presents a problem; it does not show up in our calculated ϵ_2. From the work on ZnS, we suspect that transitions at K terminating in K_2 will contribute to the E_2 peak,

TABLE VII. As in Table VI. (For CdS and CdSe.)

Region	Trans.	CdSe eV	CdSe ME	ϵ_2	CdS eV	CdS ME	Ident.
M_0 cp at	$\Gamma_6 \rightarrow \Gamma_1$	2.0	1.0 $\perp$	2.0	2.6	1.1 $\perp$	Gap
M_0 cp at	$\Gamma_1 \rightarrow \Gamma_1$	2.0	1.0 $\parallel$	2.0	2.6	1.1 $\parallel$	Gap
M_1 cp at	$\Gamma_5 \rightarrow \Gamma_3$	4.3	1.4 $\perp$	4.7	5.0	1.5 $\perp$	E_1A
M_1 cp at	$U_4 \rightarrow U_3$	5.0	0.7 $\perp$	5.2	5.7	0.8 $\perp$	E_1B
M_1 cp at	$U_3 \rightarrow U_3$	5.0	0.9 $\parallel$	5.2	5.6	0.9 $\parallel$	E_1B
M_2 cp at	$H_3 \rightarrow H_3$	6.0	3.5 $\parallel$	6.1	6.7	3.8 $\parallel$	E_0'
M_2 cp at	$M_2 \rightarrow M_1$	6.2	1.4 $\perp$	6.2	6.8	1.4 $\perp$	F_1
Region around	$K_3 \rightarrow K_2$	7.1	0.7 $\perp$		7.8	0.8 $\perp$	E_2
Region around	$K_2 \rightarrow K_2$	7.2	1.4 $\parallel$		8.0	1.5 $\parallel$	E_2
Large region including	$\Gamma_6 \rightarrow \Gamma_6$	7.9	2.4 $\perp$	7.8	8.5	2.5 $\perp$	E_1'
Very large region	$\Gamma_1 \rightarrow \Gamma_1$	7.7	2.1 $\parallel$	7.9	8.4	2.2 $\parallel$	E_1'

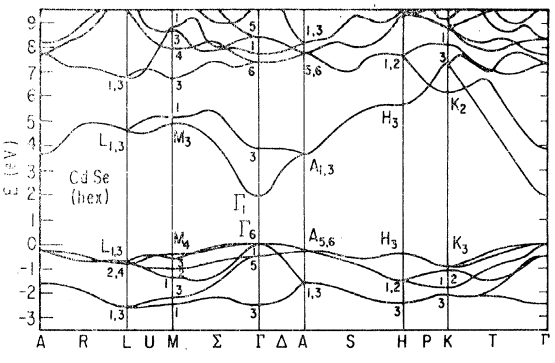

FIG. 8. Band structure of hexagonal CdSe.

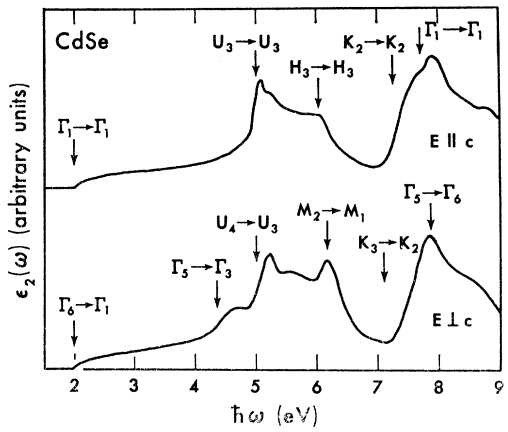

FIG. 9. Computed $\epsilon_2(\omega)$ in arbitrary units as a function of ω in eV for hexagonal CdSe.

and indeed, the energy band splittings at K are appropriate. Unfortunately these transitions merge with the too-low E_1' peak and only appear as a shoulder on the low-energy side of E_1'. This in itself is not too serious, but even if the peak were isolated, it would be a rather small peak; the matrix elements are small. On the other hand, the matrix elements are not expected to be exact. Also, the K peak suffers a false broadening and therefore weakening caused by the coarse mesh used to calculate ϵ_2 combined with the many bands cutting through each other in that region. Also, the K peak has about the same strength for both polarizations, as does the observed E_2 peak. The only other possibility in these calculations for the E_2 peak would be the transitions at and near H. However, this splitting is much to small, and the matrix elements for $\perp$ polarization are much smaller than those for $\parallel$ polarization. Also, we see in Fig. 10 that the dip before the E_2 peak for $\parallel$ polarization would thereby be filled in. For these reasons, we associate E_2 with transitions in the region of K.

The E_1' peak, as in ZnS, presents no problem, although it is too low. As before, the peak for $\perp$ polarization is associated with the transitions $\Gamma_5 \rightarrow \Gamma_6$, and that for $\parallel$ polarization is associated with $\Gamma_1 \rightarrow \Gamma_1$ (second Γ_1). The contributing regions are large and are centered about the Δ axis, extending farther toward the P axis than the U axis. Also, there is some contribution from near L, especially for $\parallel$ polarization. For both the calculation and the data, the peak for $\parallel$ polarization is 0.2 eV higher than the peak for $\perp$ polarization.

At even higher energy is found the structure labeled F_3. Some data show it as a peak and some as a shoulder. Our calculated ϵ_2 seems to show some evidence for this peak, but it is difficult to determine where in the zone it comes from. For $\perp$ polarization the peak seems to come from the B face beginning close to Δ and ending somewhat farther away from P. The fourth and fifth conduction bands are involved. For $\parallel$ polarization, the peak seems to come from the region of M; the final state is the fourth conduction band.

Reference 9 presents an OPW calculation of the band structure of CdS at special points in the zone. This work agrees well with our results; usually better than $\frac{1}{2}$ eV for the important transitions. This work also computes a band structure by a pseudopotential technique that is somewhat different from ours. This band structure is quite different from ours and is quite different from the OPW calculation. The chief reason for this difference is that the E_0' peak was used to give the $\Gamma_6 \rightarrow \Gamma_6$ splitting. This assignment of the E_0' peak is certainly not correct.

Difficulty is encountered in an attempt to fit the optical data[23] of both cubic and hexagonal CdS using a single set of form factors. The form factors used here for CdS give cubic and hexagonal band structures that obey quite well the Birman correspondence. On the basis of the Birman correspondence, one would expect to find the E_1 peak in cubic CdS lying approximately at the energy of the E_1A peak of hexagonal CdS. However, it is found to lie at the E_1B peak energy, 0.6 eV higher. Another problem is that the form factors used here for hexagonal CdS produce an E_2 peak that is too high and an F_1 peak that is close to the correct value. But the same form factors used for cubic CdS would produce an E_2 peak that is $\sim$1 eV too low. On the face of it, these two problems indicate that cubic CdS has a stronger antisymmetric potential than hexagonal CdS; but yet the gap and other peaks of the two structures correspond closely in energy. We have not attempted to produce a band structure of cubic CdS. More data on different samples would be helpful.

VI. DISCUSSION

Our interpretation of the optical structure of the wurtzite materials has been given in Secs. IV and V and is summarized in Tables VI and VII. This interpretation has been based on these considerations: The use of the form factors of ZnS obtained from the optical data of zinc blende has given a reliable band structure of wurtzite. The calculated $\epsilon_2(\omega)$ for ZnS and CdSe has been compared to the experimental reflectivity. The correspondences between the cubic and hexagonal Brillouin zones have been considered. For some identifications, not all of these considerations apply. In addition the spin-orbit splitting of the E_1A peak has corroborated its identification, and the interpretation of the fundamental gap is well-known from other considerations. The reliability of the band structures rests on these considerations.

It may be said of CB that it provided an interpolation procedure for the energy bands between known points.

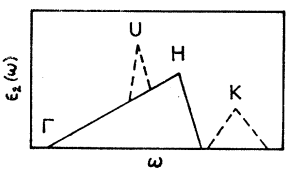

FIG. 10. Sketch for CdS or CdSe of the contribution to ϵ_2 of transitions terminating in the first and second conduction bands for parallel polarization. Energy splittings are indicated.

The general features of the band structures were for the most part already known by means of the previous EPM calculations on Ge and by other considerations. But in the case of wurtzite materials, the EPM has helped to determine the character of previously unidentified structure and has provided us with an unfamiliar band structure which has given some unexpected results. The origin of the E_1A, E_1B, and F_1 peaks has been pinpointed to well-defined locations and transitions in the zone, and the E_1' peak has been identified with a large region and specific final states. The role of dipole matrix elements in ensuring the similarity of the zinc blende and wurtzite optical structures has been understood. The E_2 peak in ZnS has been understood, and at least some of its contributing transitions in CdS and CdSe are known. The E_0' peak in CdS and CdSe has been given a tentative interpretation.

In the course of the identification of the optical structure, certain problems have arisen: the unidentified shoulder to the E_1 peak of ZnS, the uncertainty about the band structure of cubic CdS, and some uncertainty in the identification of the E_0' and E_2 peaks of CdS and CdSe. These could very well be indications of a breakdown of the EPM or an indication of an incorrect application of the EPM. On the other hand, most such problems in the past have been resolved in favor of the EPM by new experimental data. It should be noted that the problems with these materials are not solely a matter of their ionic nature. The band structure of the more ionic crystal MgO has been given very accurately by the EPM.[3] In any case, these problems will be resolved by reference to experiment. In the meantime, these band structures are the most accurate available. They will be useful in the continuing investigation of these materials.

There are several known inadequacies of the EPM as presently applied. One is the lack of an energy dependence in the form factors as discussed in CB. This causes no problem in the interpretation of optical structure. Another inadequacy is the convenient requirement that form factors be zero for $G^2 \geq 16$. However, we are able to fit the data adequately under the chosen constraints. There exists the question of why the EPM works so well. As discussed in CB, the physical nature of the Hamiltonian combined with the reference to experimental data in the course of the calculation has produced very reliable band structures. We see now that the reliability extends to the form factors in that they have been taken from zinc blende and used without modification in wurtzite. This has produced for wurtzite a band structure that is as reliable as the one for zinc blende. The fact that it has given the expected correspondences between the two zones, and even has given the correct crystal field splittings at Γ, and also at L and K, gives us confidence in the entire process. A full theoretical explanation of the success of the EPM remains to be given, although the partial explanation by means of the pseudopotential cancellation theorem has been known for some time.

The present use of the EPM to go from zinc blende to wurtzite is an indication of the usefulness of the form factors obtained. However, it should be remembered that the form factors may need to be slightly modified for more diverse usage. The validity of the form factors obtained in an EPM calculation may be tested in several ways. The form factors for the group IV elements have been compared in CB to the form factors of the model potential of Animalu and Heine.[40] Another test is in the use of the form factors of GaAs and InSb to provide a good trial potential in the calculation of the band structure of As and Sb.[4] Also, the ZnS form factors have been used in obtaining those for MgO.[3] Our form factors are appropriate for a particular valence band potential, which is one cause of difference with the model potential, and has been judged to give a negligible effect in the work on As, Sb, and MgO. Furthermore, the fact that our form factors are required to be zero for $G^2 \geq 16$ gives cause for a difference in both cases. Another reason for difference between sets of form factors is the somewhat subjective nature of the process of choosing the empirical form factors. The emphasis in the present work is upon fitting optical structure over a wide range of energy. None of these reasons gives cause for a significant change in form factors upon going from zinc blende to wurtzite.

ACKNOWLEDGMENTS

We thank Professor J. C. Phillips for helpful comments. One of us (T.K.B.) would like to express his gratitude for the hospitality extended to him at the Cavendish Laboratory where the final draft of this manuscript was written.

[40] A. O. E. Animalu and V. Heine, Phil. Mag. 12, 1249 (1965).